Journal of Thermal Science Vol.22, No.6 (2013) 592–599

DOI: 10.1007/s11630-013-0667-1 **Article ID: 1003-2169(2013)06-0592-08**

Experimental Investigation of Effects of Distributed Riblets on Aerodynamic Performance of a Low-speed Compressor

MA Hongwei*, WEI Wei

National Key Laboratory of Science and Technology on Aero-Engines, School of Energy and Power Engineering, Beihang University, Beijing, 100191, China

It is well known that riblet applied on compressor blades is a promising flow control technique. However, detailed investigation of its effects on the flow field of turbomachinery is rare in existing literatures. This paper presents a detailed experimental investigation of effects of distributed riblet on the flow field of an axial compressor isolated-rotor stage. The research was performed in a large-scale facility respectively with two configurations, including grooved hub, and grooved surface on both hub and partial suction surface. The riblet film is rectangle grooved type with a height of 0.1 mm. The flow field at 10% chord downstream from the cascade trailing edge was measured using a mini five-hole pressure probe and a total pressure probe. The testing was conducted at several operational points under two reduced rotational speeds. Stagnation pressure loss in rotational frame was calculated and compared with the control test in which a smooth film was applied to the corresponding position. Results show that with the grooved hub configuration at the design operation point of the lower rotational speed, the riblet film provides an obvious improvement of a 48% reduction of total pressure loss in rotational frame. Also, a distinct weaken hub corner vortex was identified. In the meantime, there exists a deviation of flow angle about 5 degrees at 20%-80% span which previously was not considered to be the affected region.

Keywords: distributed riblet, large-scale compressor, hub corner vortex, loss reduction.

Introduction

It was well known that the surface with specially-designed streamwise grooves named riblet could reduce flow drag compared with the smooth surface. Many researchers have investigated the effects under different configurations of various scales, including academic, industrial settings. There already exist plenty of well-developed reviews [1]. A320 flight tests showed that the fuel saving of 1%~1.5% could be obtained while the plane was dressed with riblet films [2]. From the viewpoint of academic researches, Gallagher, Thomas [3], and Choi [4] considered that thickening of the sub-layer due to the riblet could lead to drag reduction. Bacher & Smith [5] found that the flow within the riblet was remarkably slow and exhibited poor lateral spreading behavior; as a result, they made a conclusion that the drag reduction was attributed to the secondary vortices formed in the grooves. Gong et al [6] observed that the average turbulent kinetic energy and peak values of the turbulent kinetic energy components in the boundary layer on a flat plate were reduced. Wang et al [7] found that the non-dimensional spacing of neighbor low-speed streaks was reduced by 20% which should be a vital factor of

Received: June 2013 Hongwei MA: Professor
This work was funded by the National Natural Science Foundation of China, Grant No. 51161130525 and 51136003, supported by the 111 Project, No. B07009.

Nomenclature

STH	with smooth film	*Yaw*	flow angle at outlet (degree)
HR	with riblet on hub	*Beta*	pitch angle at outlet (degree)
HBR	with riblet on hub and partial suction side	*cvz*	V_{a1} /U_{tip}, axial flow coefficient
RPM	rotational speed (r/min)	*cpt*	(Pt_1–Pt_0) /*Dp*, *Pt* coefficient
N	Reduced rotational speed (r/min)	*cps*	(Ps_1–Ps_0) /*Dp*, *Ps* coefficient
Dp	dynamic pressure at inlet (Pa)	**Greek letters**	
Ps	static pressure at outlet (Pa)	ξ	relative total pressure loss coefficient
Pt	total pressure at outlet (Pa)		normalized by *Dp*
V	velocity (m/s)	**Subscripts**	
U_{tip}	tangential velocity of blade tip (m/s)	0	compressor inlet
cva	V_0 / U_{tip}, axial velocity coefficient at inlet	1	compressor outlet
cp	(Ps_1–Ps_0) /*Dp*, static pressure rise coefficient	t	tangential
W2u	V_t in RF at outlet (m/s)	a	axial

drag reduction. Although a uniform conclusion of the mechanism of the drag reduction by riblet is not achieved, more and more practical application [8-11] have been investigated, and promising results were reached. Matthias and Leonhard [8] carried on an experimental investigation of a highly loaded compressor cascade, a reduction of 5% of the total pressure loss coefficient was observed, within the Reynolds number range from 1.5E5 to 11.0E5. Karsten et al [9] investigated effects of the machined riblet structures, which are fabricated by grinding and laser machining, on the performance of a compressor cascade. They considered that undersized groove height and tip angle which is not small enough as design should be responsible for the low loss reduction value (1.6%). After an improvement of the machining process, a total pressure loss reduction up to 7.2% could be reached [10]. Christopher et al [11] summarized the advances in manufacturing of riblet on compressor blades. Applications of riblet on industrial products recently are limited by the machining method, and it's easy to understand the difficulty of manufacturing uniform riblet on continuously variable surfaces. As a result, more and more researches are carried on with numerical simulation method. For example, James and David [12] suggested that optimized height of the riblet might have to grow with downstream distance from the results of their LES simulations. Nevertheless, research of effects of riblet on a real compressor test rig is rare. Ma et al. [13] investigate the effects of the same kind of riblet utilized in this article on the unsteady flow field at the outlet of an axial fan. Positive result has been observed through detailed steady and unsteady measurement.

This paper presents an experimental investigation of effects of distributed riblet on the flow field of an axial compressor isolated-rotor stage.

Experimental Procedure

Experimental Facility and Test Technique

The experimental investigation was carried out in a large-scale compressor facility, as shown in Figure 1, in National Key Laboratory of Science and Technology on Aero-Engines at BUAA. An isolated rotor is deployed to provide the research environment. The compressor is operated at four operational points, (cva=0.55, near-stall point; 0.60, mid-operating point; 0.65, design point; 0.77, large massflow point), under two reduced rotational speed of 700 RPM and 900 RPM with a rotation speed drift of 0.5RPM. The diameter of the compressor casing is 1 m, while the hub-to-tip ratio is 0.6. The isolated-rotor stage comprises 17 blades with a tip clearance of 3 mm. The rotor blades with C4-series airfoil are designed in terms of the free vortex law. The blade camber angle is 26.5 degrees, and the blade stagger angle is 33.4 degrees. The measurements were taken at the Reynolds number of $4.4\sim5.6\times10^5$ based on the blade chord and the inlet velocity.

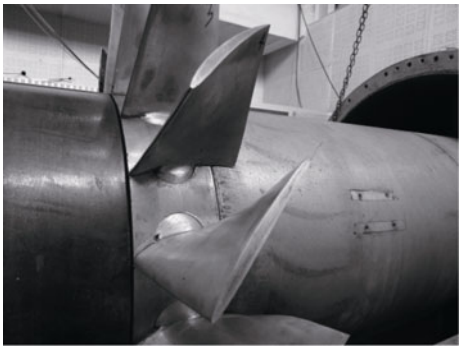

Fig. 1 The research isolated-rotor

Figure 2 illustrates the sectional view of the riblet. The riblet film is rectangle grooved type with a height of 0.1 mm. Most researches on riblet recently concern a lot about the manufacture process [11]. Some researchers [8-10] preferred precision machining directly on the blades, while others [13] chose to apply customized films on the immersed surfaces. In this research, plastic sheet with a uniform thickness was machined by compression moulding method. The total thickness, including adhesive coating, is 0.24 mm, which means 0.15% of the pitch at mid-span or 0.11% of the passage height. It is rational to neglect the blockage of this film. Typical parameter s^+ equals 38, while h^+ is 4, which is a compromise of feasibility and performance.

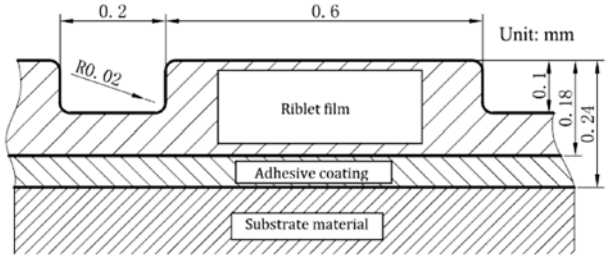

Fig. 2 Riblet distributed on the blades

The configurations explored include a) grooved hub and b) grooved surface on both hub and partial suction surface, as shown in Figure 3. Another case with a smooth film is referenced as the baseline. In both of the riblet configurations, direction of the micro-channels on the riblet film was aligned parallel with the axial direction. In the configuration b, riblet film was also applied to the lower one third of the suction side surface. It should be noted that the film was extended to the pressure side from the leading edge to 10% axial chord downstream.

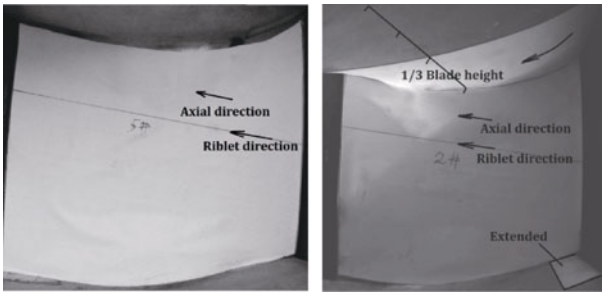

(a) Riblet configuration a (b) Riblet Configuration b

Fig. 3 Configurations of riblet distribution

The plane at 10% chord downstream from the rotor trailing edge was measured using a mini five-hole pressure probe and a total pressure probe at 45 spanwise stations. The five-hole probe has a conical head with a diameter of 2 mm. Its measurement uncertainties of angles are less than 1° while the uncertainty of total pressure is less than 1.0%.

The total pressure probe has one pressure tap with a diameter of 2.2 mm. The initial yaw angle of each radial station was calculated from the data from the measurement of five-hole probe. Sampling number per station of total pressure probe was 200k with a sampling rate of 20k.

A PXIe data acquisition system provides a high level of performance with synchronization technology. The measurement was programed in the environment of LabVIEW. During the experiment, the method of software triggering is chosen rather than phase-locked sampling technique, with which continuous signal is recorded. The response time of optical trigger subsystem is less than 1E-5 second. The data reduction method utilized in this paper could refer to the literature [14].

Result and Discussion

Figure 4 gives the performance maps of the three investigated cases at two reduced rotational speed. An improvement could be observed at the operational points of near-stall and large massflow condition at lower rotational speed. As the rotational speed increases, an evident improvement also appears at mid-operating condition. As known, the performance of a compressor test rig always utilizes static pressure taps on the casing at inlet and outlet to evaluate the static pressure rise or ratio (high-loaded compressor); nevertheless, the pressure taps cannot be accurate enough to show the area-averaged static pressure at the outlet. As a result, more detailed measurement was performed to assure the precision.

Overall performance comparison

Figure 5 illustrates the mass-averaged ξ at two reduced rotational speed.

$$\xi = (\frac{1}{2}\rho U_{Span}^2 - \frac{1}{2}\rho W_2^2 - P_S) / D_P \qquad (1)$$

The Eq. (1) gives the definition of total pressure loss in the rotational frame, where W_2 is the relative velocity at the outlet. U_{Span} in the Eq. gives the distribution of tangential velocity of the rotor.

Both the riblet configurations exert positive effects on the performance of the compressor as shown in Figure 5a. However, the two configurations show different tendency along with the growth of the axial velocity coefficient. Relative total pressure loss of the configuration HR decreases with cva, while HBR has a peak loss reduction at the mid-operating point. As cva increases, the included angle between the flow and the riblet would be less, which contributes to more loss reduction. However, the configuration HBR appear to introduce negative impact

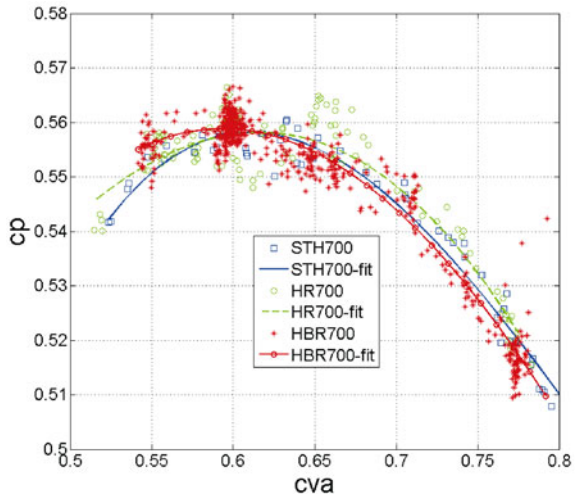

(a) *N*= 700r/min

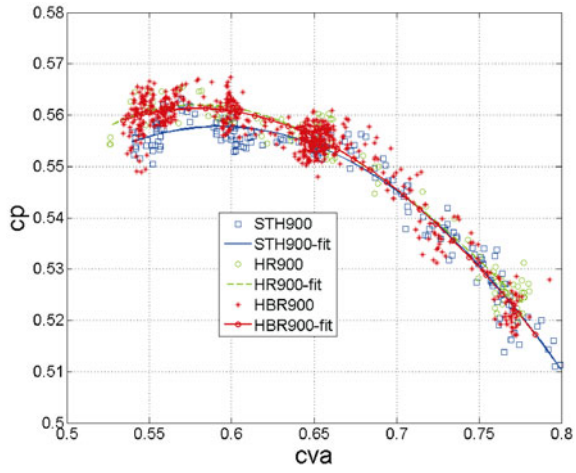

b) *N*= 900r/min

Fig. 4 Performance map

on the performance while cva is greater than 0.6. To put it another way, the additive riblet film on suction side of the blade should account for the further reduction of loss at near-stall condition and weaken positive effects at design point.

The maximum loss reduction (48%) locates at the large massflow point while configuration HR is applied. The compressor operates around mid-operating and design point more frequently, as a result, 28% would be a more suitable typical value.

While the compressor operates at the higher N, as shown in Figure 5b, the riblet film on the suction side of the blade obviously impose a negative effect on the performance. In addition it is worth noting that the loss reduction effect almost disappears at the near-stall point.

Figure 6 demonstrates the area-averaged axial velocity coefficient, namely the flow capacity. The case HR shows small positive effects to the compressor.

Figure 7 demonstrates the area-averaged static pressure coefficient of the three cases at two reduced rotational speed. The rotational speed leads a main impact on the performance of static pressure rise. In Figure 7a, configuration HBR shows an improvement of compression capacity and the maximum rise (10.4%) is marked.

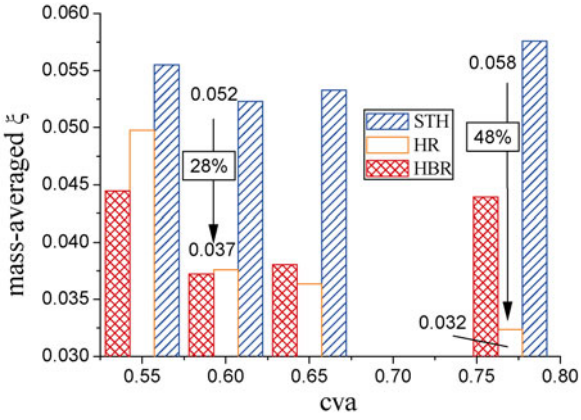

(a) *N*= 700r/min

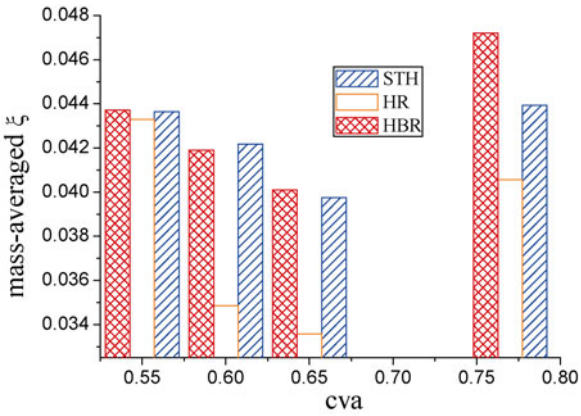

(b) *N*= 900r/min

Fig. 5 Mass-averaged ξ in RF at outlet

Spanwise distribution of ξ in RF

Figure 8 shows the spanwise distribution in rotational frame. Three operational points, including a) N= 700 r/min, cva= 0.60, b) N= 700 r/min, cva= 0.77, c) N= 900 r/min, cva= 0.60, are demonstrated. In the following paragraphs, these representative operational points would be discussed.

At the operational point a, a small but clearly depression of loss could be observed below 10% blade height. The maximum effected region is located at 10% to 80% blade height, which could be also observed at the operational point b. Nevertheless, at the large massflow point the positive impact at upper-half passage turns weaken comparing with that of mid-operating point. Figure 8c gives the comparison of spanwise distribution of ξ at N= 900r/min. The configuration HBR throws negative impact at 8% to 20% blade height.

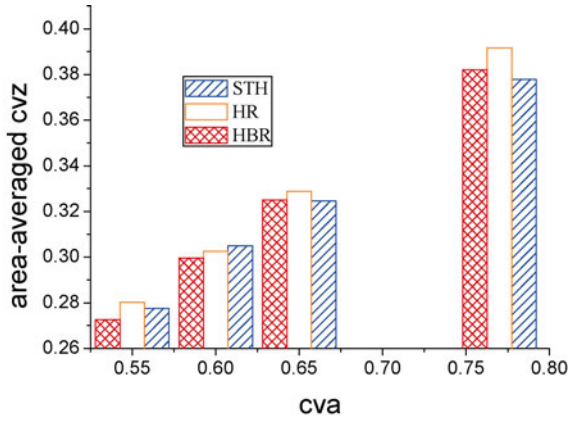

(a) N= 700r/min

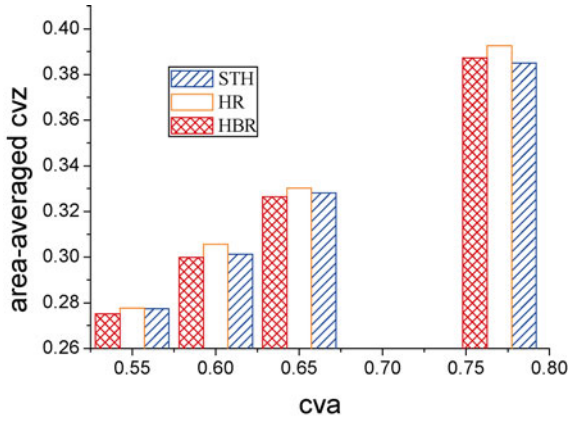

b) N= 900r/min

Fig. 6 Area-averaged cvz at outlet

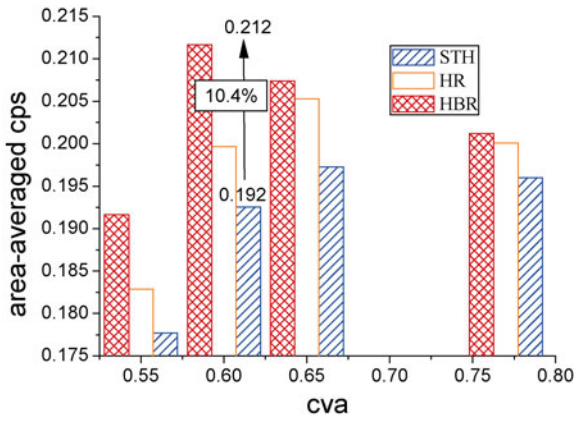

(a) N= 700r/min

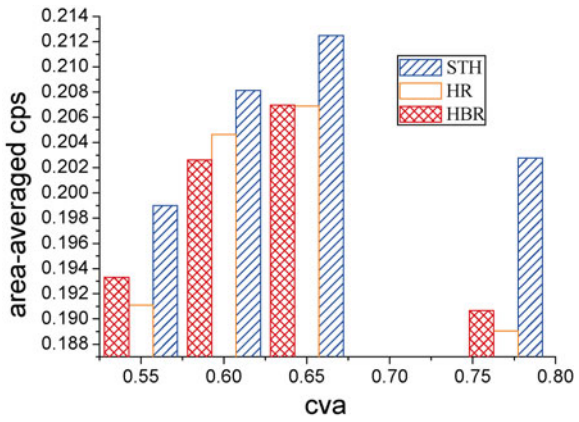

(b) N= 900r/min

Fig. 7 Area-averaged cps at outlet

What's interesting in Figure 9a is that the configuration HR would affect the lower 40% passage, while HBR offset the whole spanwise distribution, which is in accord with the riblet distribution. However, in higher reduced rotational speed, both configurations of riblet would impact the 30% to 70% blade height.

Spanwise distribution of cps

Considering Eq. (1), the contribution of loss reduction could be decomposed into two main factors, i. e., parameter Ps and W_2. In order to analysis the mechanism of loss reduction, Figure 10 illustrates the spanwise distribution of Yaw, W2u, and Beta, while cva= 0.60, N= 700 r/min. The influence of Beta could be ruled out as the small variation. W_2 of the three cases almost stay unchanged which is not necessary to display. Figures 10a and 10b shows that the flow angle at the outlet of the rotor is affected, which contribute to a larger W_2 at the outlet.

Combined effects could be obtained from Figure 9a and Figure 10a; configuration HR gives larger cps below 40% blade height and larger flow deviation angle between 20% to 80% span. At the same time, HBR gives larger cps across the whole blade span and small flow deviation angle. This could explain the same loss reduction value while cva= 0.60, N=700 r/min.

In the previous published literatures, a typical loss reduction of 12% with riblet was considered to be perfect. The loss reduction of 48% obtained in this research, however, is not contradictory to that result. The riblet film applied not only modifies the boundary layer behavior on the hub, but also creates positive effects towards the hub corner separation from the leading edge of this rotor.

Figure 11 illustrates the contours of cpt for the three cases. The low cpt region marked in Figure 11a is clearly improved in the riblet configurations. Besides that, the area affected by the corner separation is reduced, which could be observed in Figures 11b and 11c.

Conclusions

This paper presents a detailed experimental investigation on effects of two riblet configurations on the flow

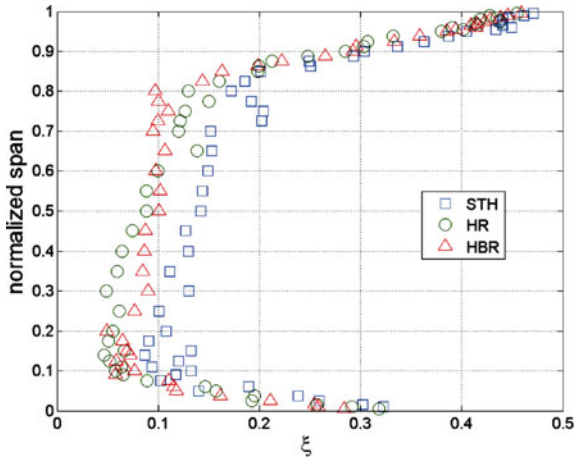

(a) N= 700r/min, cva= 0.60

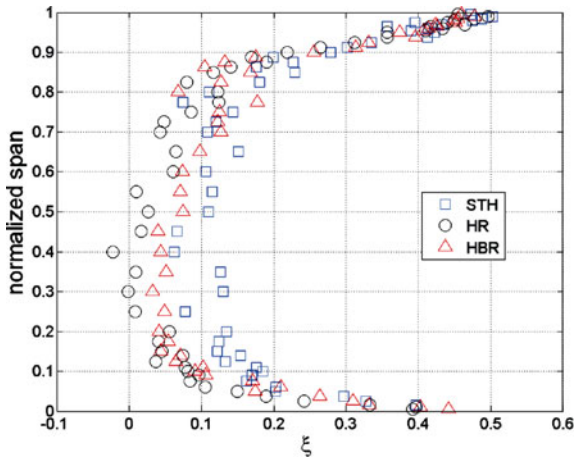

(b) N= 700r/min, cva= 0.77

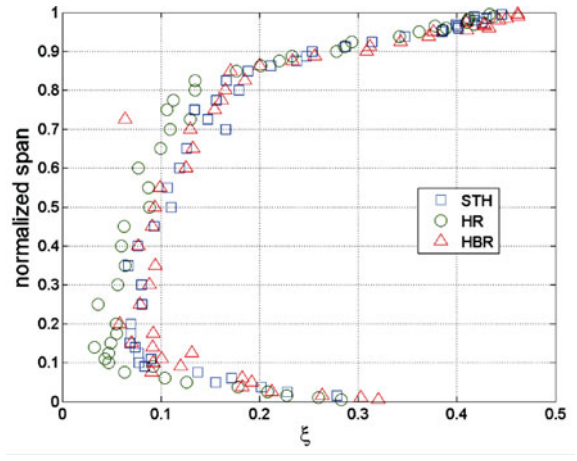

(c) N= 900r/min, cva= 0.60

Fig. 8 Spanwise distribution of ξ at outlet

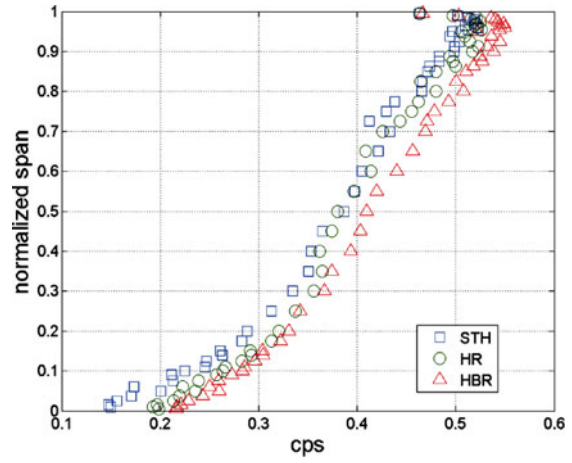

(a) N= 700r/min, cva= 0.60

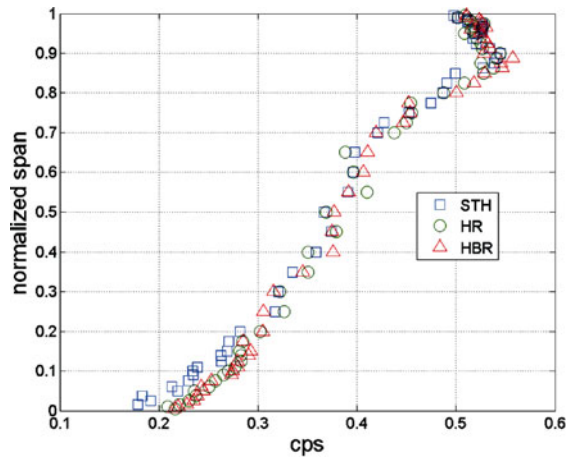

(b) N= 700r/min, cva= 0.77

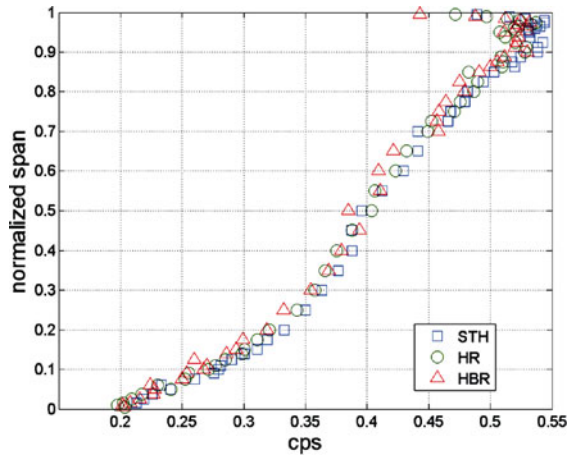

(c) N= 900r/min, cva= 0.60

Fig. 9 Spanwise distribution of cps at outlet

field of an axial compressor isolated-rotor stage. Several conclusions are listed as follows:

(1) The riblet applied on the hub has a better loss reduction effect than the configuration b in this test setting. The maximum loss reduction (48%) locates at the large massflow point, N= 700r/min, in the HR configuration.

(2) The riblet not only modifies the boundary layer behavior on the hub, but also create positive effects towards the hub corner separation from the leading edge of this rotor.

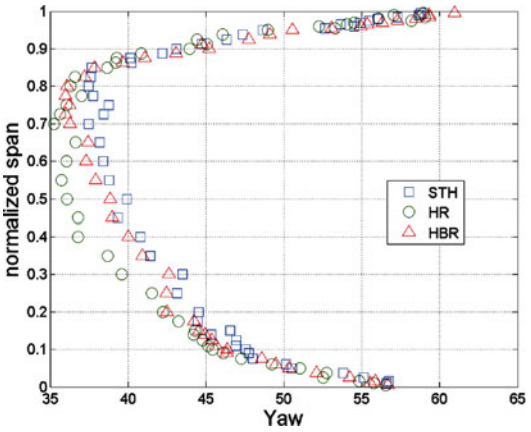

(a) Yaw

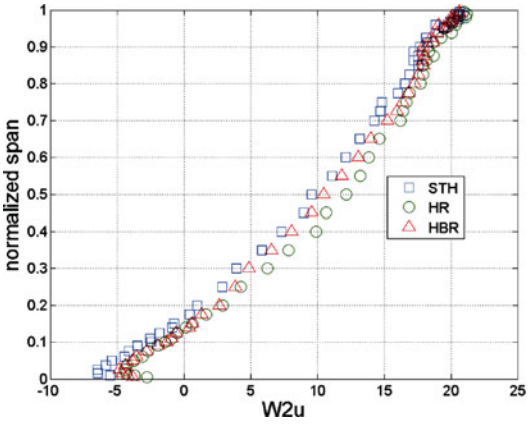

(b) W2u

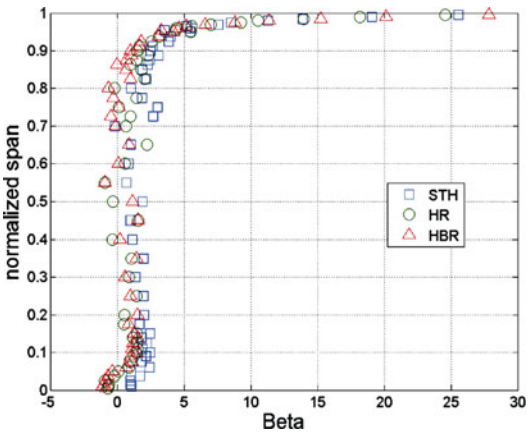

(c) Beta

Fig. 10 Spanwise distributions of Yaw, W2u, and Beta cva= 0.60, N=700r/min

(3) The loss reduction characteristic of the riblet film is strictly limited by the rotational speed of the rotor, which indicates that the cross section and install direction of riblet has to be carefully chosen for the design point.

(4) In order to improve the performance of a compressor, further study should be carried out to understand its complex flow field of a research compressor. It would be better to distribute the riblet on some critical area for more improvement.

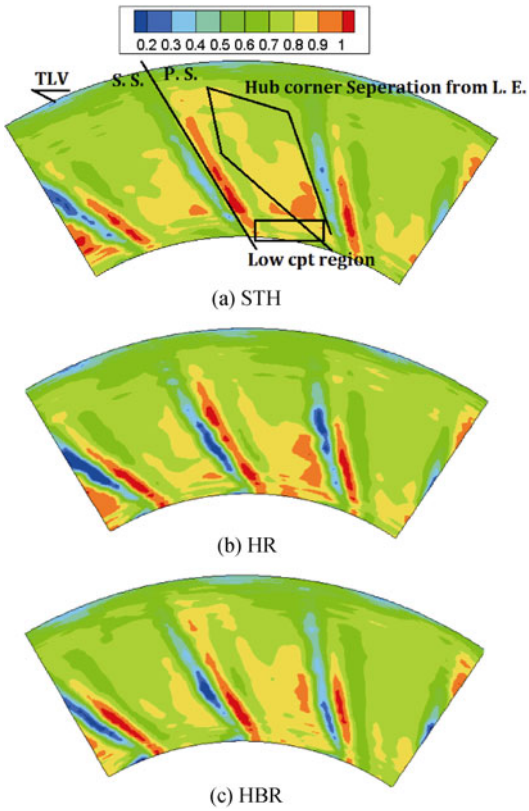

Fig. 11 Contours of cpt, *N*= 700r/min, cva= 0.60

Acknowledgement

This work was funded by the National Natural Science Foundation of China, Grant No. 51161130525 and 51136003, supported by the 111 Project, No. B07009.

References

[1] Viswanath, P. R., Riblets on Airfoils and Wings: A Review, 30th AIAA Fluid Dynamics Conference, 1999, Norfolk, VA, AIAA-99-3402.

[2] Marec, J.P., Drag Reduction: a Major Task for Research, CEAS/DragNet European Conference, Potsdam, Germany, 2000.

[3] Gallagher, J. A., Thomas, W., Turbulent Boundary Layer Characteristics Over Streamwise Grooves, AIAA 84-0347, Seattle, USA, 1984,.

[4] Choi, K.S., Near-Wall Structure of a Turbulent Boundary Layer with Riblets, Journal of Fluid Mechanics, 1989, vol. 208, pp,417–458.

[5] Bacher, E. V., Smith, C. R., A Combined Visualization-Anemometry Study of the Turbulent Drag Reducing Mechanisms of Triangular Micro-groove Surface Modifications, 1985, AIAA 85-0548, Boulder, USA.

[6] Gong, Wuqi, et al, Experiment Study on the Mechanism

of Riblets Drag Reduction, Journal of Engineering Thermophysics, 2002, 23(5): 579–582.

[7] Wang, Jinjun, et al, Experiment Study on the Turbulent Boundary Layer Flow over Riblets Surface, Journal of Mechanics, 2000, 32(5): 621–626.

[8] Matthias, B., Leonhard, F.: Effects of Riblet on the Loss Behavior of a Highly Loaded Compressor Cascade, Proceedings of ASME Turbo Expo, 2002, Netherlands, GT-2002-30438.

[9] Karsten, O., Joerg, R. S., Exploratory Experiments on Machined Riblets on Compressor Blades, Proceedings of FEDSM, 2006, FEDSM-2006-98093, Miami, USA.

[10] Karsten, O., Joerg, R. S., et al., Exploratory Experiments on Machined Riblets for 2-D Compressor Blades, Proceedings of IMECE, 2007, IMECE-2007-43457, Seattle, USA.

[11] Christoph, L., Berend, D., Recent Advances in Manufacturing of Riblets on Compressor Blades and Their Aerodynamic Impact, Proceedings of ASME Turbo Expo, 2012, Denmark, GT-2012-69067.

[12] James, S. S., David, B. G., Direct Numerical Simulations of Riblets to Constrain the Growth of Turbulent Spots, Journal of Fluid Mechanics, vol. 668, pp.267–292, (2011).

[13] Ma, H., Guo, J., Effects of a Kind of Non-smooth Blade on the Unsteady Flow Field at the Exit of an Axial Fan, Journal of Thermal science, pp.200–205, (2006).

[14] Ma, H., Jiang H., Three-dimensional Turbulent Flow Field at the Exit of an Axial Compressor Rotor Passage in Both Design and Near Stall Conditions, Journal of Engineering Thermophysics, vol. 18, pp.153–158, (1997).